Bioinspired Intermittent Control of a Miniature Autonomous Blimp for Tracking a Moving Target

Rachel J. Suitor[1,2], Donald Sofge[1], and Derek A. Paley[2]

[1]*U.S. Naval Research Laboratory, Washington, DC, USA;* [2]*University of Maryland, College Park, MD, USA*

Abstract—**Intermittent actuation for autonomous systems inspired by biological locomotion can leveraged for swarming platforms tasked with underwater localization and tracking. This paper presents the design of a control strategy for a neutrally buoyant vehicle tracking a moving target using intermittent actuation. Tracking a time-varying reference with intermittent actuation is presented using state-feedback control for the decoupled 1-DOF cases of vertical motion and rotational motion about the vertical axis. Experimental results from tests on the miniature autonomous blimp platform demonstrate the control strategy on a neutrally buoyant vehicle.**

Index Terms—**Intermittent actuation, autonomous tracking, nonlinear dynamics**

I. INTRODUCTION

Intermittent motion is frequently observed in biological locomotion. In many species, locomotion patterns alternate between active and passive periods [1], [2]. This allows for animals to conserve energy while traversing their environments while also benefiting the animal's sensory biology for improved perception and decision making [2]–[4] Such benefits also include cohesion of collective animal motion [2], which can be leveraged for bioinspired collective motion of multi-agent systems [4]–[7] reducing both communication and control energy costs [8]. Multi-agent autonomous platforms for underwater localization and tracking can provide significant advantages over single agent or non-autonomous methods such as greater spatiotemporal coverage, increased data collection, and the capability for cooperative sampling strategies [5]. The underactuated autonomous Lagrangian drifter platform, Driftcam, in [9], [10], for multi-agent *in situ* observation of marine life, utilizes buoyancy-driven depth control to remain minimally invasive to the ecosystem. The neutrally buoyant underwater vehicle in [9] uses a continuous control effort. Expanding on that work, [11] proposes a discrete-time tracking control strategy for the same drifter platform.

The platform used for this work is a lighter-than-air miniature autonomous blimp (MAB) [12], [13], shown in Fig. 1, which is a low-cost, neutrally buoyant platform for testing algorithms on single- or multi-agent systems [14]. The full 6-DOF dynamic model for the MAB, discussed in Section II, is derived from the same kinematics as the dynamics model for the Driftcam [10], [12], [15]. Additionally, the blimp has

low-power thrust relative to its size that make it necessary to consider the aerodynamics in the model, which is more similar to modeling underwater vehicles than it is to modeling higher-thrust aerial systems such as quad-copters [12].

This work builds on the idea of discrete-time tracking control for a neutrally buoyant robotic platform, presenting simulated and experimental results for a single vehicle implementing an intermittent actuation algorithm for target tracking. The specific contributions of this paper are a control strategy for tracking a time-varying target reference using intermittent actuation with a linear tracking state for vertical motion and with a nonlinear tracking state for rotational motion. Simulated and experimental results demonstrate implementation of intermittent actuation on a miniature autonomous blimp platform.

The outline of the paper is as follows. Section II describes the dynamics of the miniature autonomous blimp vehicle. Section III presents and analyzes a theoretical control method for tracking a time-varying reference with intermittent actuation. Section IV presents experimental results. Section V summarizes the paper and ongoing work.

II. SYSTEM BACKGROUND

A. Platform description

The miniature autonomous blimp (MAB), shown in Fig. 1, is a lighter-than-air aerial platform comprised of a 36 inch-diameter mylar envelope with an attached gondola for the motor-propeller system and onboard electronics. The MAB is equipped with a camera, an IMU, and a range sensor measuring the vertical time-of-flight. An onboard processor streams sensor data to the ground station over Wi-Fi. Feedback control is computed at the ground station and transmitted to the blimp's microcontroller to actuate the motors [13], [16]–[18]. The existing control architecture for the MAB includes a low-level PID for stabilized automatic flight.

B. Blimp dynamics and control

This section describes an idealized model of the dynamics for a blimp. The idealized 6-DOF model for the rigid-body blimp can be described with $\mathbf{M}\dot{\boldsymbol{\nu}} + \mathbf{D}(\boldsymbol{\nu})\boldsymbol{\nu} + \mathbf{g}(\boldsymbol{\eta}) + \mathbf{g}_0 = \boldsymbol{\tau}$, where $\boldsymbol{\nu} = [u,\ v,\ w,\ p,\ q,\ r]^T$ is a vector of velocities, $\boldsymbol{\eta} = [x,\ y,\ z,\ \phi,\ \theta,\ \psi]^T$ is a vector of positions and Euler angles, and $\boldsymbol{\tau} = [X,\ Y,\ Z,\ K,\ M,\ N]^T$ is the vector of forces and moments [12], [16]–[18]. The matrices $\mathbf{M}$ and $\mathbf{D}(\boldsymbol{\nu})$ are the rigid-body inertia and damping, respectively. The vectors $\mathbf{g}(\boldsymbol{\eta})$ and $\mathbf{g}_0$ represent the generalized gravity and buoyancy forces
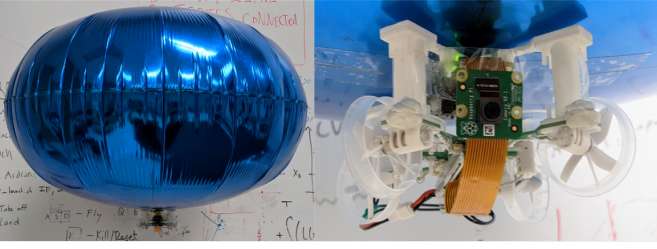
Fig. 1: The miniature autonomous blimp vehicle (GT-MAB) as described in [13]. Left: an inflated helium envelope with the gondola attached to the bottom. Right: a close-up of the gondola housing the onboard processing and sensors.

on the system. The constant parameters drag D, mass m, and moment of inertia I_G are from [16] and are used to compute the inertia and damping matrices.

We define two reference frames to describe the motion of the MAB in 6 degrees of freedom (DOF): An inertial frame I defined with origin $O(x_i, y_i, z_i)_I$, and a body-fixed frame B with origin at the center of gravity of the vehicle $(x, y, x)_B$. The body frame axes are defined with the positive directions as x forward, y left, and z up (FLU).

The blimp flight controller contains a set of nested PID control loops [13] designed to stabilize oscillations and achieve continuous velocity and waypoint tracking [18]. An open source API for the GT-MAB blimp provides methods for retrieving the onboard state and sensor information and for updating the controller inputs. Access to the onboard controller is available through two methods. The first method accepts desired local frame rotation states $[\phi_d, \theta_d, \psi_d]_B$ and uses nested PIDs to compute the necessary control forces while the second method accepts a vector of desired control forces directly. The input forces are then used to compute commands for the appropriate motors. This work focuses on the decoupled 1-DOF cases of vertical motion, $z \in \mathbb{R}$, and rotational motion about the z-axis, $\theta \in \mathbb{R}$.

III. CONTROL FOR INTERMITTENT REFERENCE TRACKING

This section presents an intermittent actuation control strategy with one degree of freedom for tracking a target reference signal for (1) vertical motion, $z \in \mathbb{R}$ with second-order dynamics

$$m\ddot{z} = -D\dot{z} + u(t) \tag{1}$$

and (2) rotation about the vertical axis, $\theta \in \mathbb{R}$ with second-order dynamics

$$I_g\ddot{\theta} = -D\dot{\theta} + u(t). \tag{2}$$

The intermittent actuation algorithm has a short burst phase with active control followed by a longer, passive coast phase. The burst phase control, derived in the following subsections, is designed to converge to the target reference in a minimum number of burst-coast cycles. Proximity to the target is evaluated at the end of the coast phase. If the proximity is not within a specified threshold, then the algorithm continues

through the next burst-coast cycle and reevaluates. If the proximity is within the specified threshold at the end of the coast phase, then the target is marked as reached and the target is updated for the next burst-coast cycle. After setting a new target, the proximity is checked so that if the target is within the proximity threshold the burst phase is skipped and only the coast phase is executed for that cycle. For a moving target, assume that the target velocity doesn't exceed the maximum velocity of the blimp. For the constant target case, the algorithm does not include the coast-only cycle, and instead the full burst-coast cycle is used for each time step.

The following subsections present the derivation of the intermittent control strategy for the general case of tracking a moving target for the vertical and rotational motion. Then the specific case of tracking a constant target is presented for vertical and rotational motion, along with simulation results.

A. Vertical reference tracking with intermittent actuation

Let $\mathbf{z} = (z_1, z_2) = (z, \dot{z})$. The state dynamics for the 2nd-order linear system in (1) are

$$\dot{z}_1 = z_2 \tag{3}$$

$$\dot{z}_2 = -\frac{D}{m}z_2 + \frac{1}{m}u, \tag{4}$$

where u is a control input. Let $r = r(t)$ denote a continuously differentiable time-varying reference signal with bounded derivatives tracked by vertical position, and let $\mathbf{e} = (e_1, e_2) = (z - r, \dot{z} - \dot{r})$ denote the tracking error.

The continuous-time error dynamics are

$$\dot{e}_1 = e_2 \tag{5}$$

$$\dot{e}_2 = -\frac{D}{m}z_2 + \frac{1}{m}u - \ddot{r} \tag{6}$$

and the state-space form is

$$\dot{\mathbf{e}} = \mathbf{f}(\mathbf{e}, u) = \begin{bmatrix} e_2 \\ -\frac{D}{m}z_2 + \frac{1}{m}u - \ddot{r} \end{bmatrix}. \tag{7}$$

The open-loop error system

$$\mathbf{f}(\mathbf{e}^*, 0) = \begin{bmatrix} e_2 \\ -\frac{D}{m}z_2 - \ddot{r} \end{bmatrix} = \begin{bmatrix} z_2 - \dot{r} \\ -\frac{D}{m}z_2 - \ddot{r} \end{bmatrix} \tag{8}$$

is not easily linearized at an equilibrium point for stability analysis. However, $\dot{r}$ and $\ddot{r}$ are bounded so we instead consider the linear open-loop state dynamics $\dot{\mathbf{z}} = A_0\mathbf{z}$, where

$$A_0 = \begin{bmatrix} 0 & 1 \\ 0 & -\frac{D}{m} \end{bmatrix}. \tag{9}$$

The eigenvalues are $\lambda_1(A_0) = 0$ and $\lambda_2(A_0) = -D/m$, therefore the open-loop state dynamics are marginally stable. It follows that the open-loop error system is marginally stable and bounded.

Choosing $u = u(v)$ to feedback linearize (7) yields

$$u(v) = m\left[\frac{D}{m}z_2 + \ddot{r} + v(t)\right], \tag{10}$$

where $v(t) = -K\mathbf{e}(t)$ is a constant linear feedback control and $K = [K_1 \ K_2]$ are positive control gains.

Substituting (10) into (6) yields the following linearized state-space form for the continuous closed loop error system:

$$\dot{\mathbf{e}} = A\mathbf{e} + Bv = \tilde{A}\mathbf{e}, \tag{11}$$

where $\tilde{A} = A - BK$ and

$$A = \begin{bmatrix} 0 & 1 \\ 0 & 0 \end{bmatrix} \text{ and } B = \begin{bmatrix} 0 \\ 1 \end{bmatrix}. \tag{12}$$

Thus,

$$\tilde{A} = \begin{bmatrix} 0 & 1 \\ -K_1 & -K_2 \end{bmatrix}. \tag{13}$$

where the positive control gains K_1 and K_2 are chosen to make $\tilde{A}$ Hurwitz. Since the trace of $\tilde{A}$ is negative and the determinant is positive, its eigenvalues $\lambda_{1,2}(\tilde{A})$ lie in the left half of the complex plane.

This system is controllable because $\mathcal{C} = [B, \ AB]$ is full rank: i.e.,

$$\mathcal{C} = \begin{bmatrix} 0 & 1 \\ 1 & 0 \end{bmatrix}. \tag{14}$$

The solution to the linearized error system (11) at time t is

$$\mathbf{e}(t) = e^{At}\mathbf{e}(t_0) + \int_{t_0}^{t} e^{A\tau} Bv(t-\tau)d\tau, \tag{15}$$

where the matrix exponential is

$$e^{At} = I + At + \frac{A^2 t^2}{2!} + \dots \tag{16}$$

Since $A^2 = 0$, we have

$$e^{At} = I + At = \begin{bmatrix} 1 & t \\ 0 & 1 \end{bmatrix} \tag{17}$$

Suppose the input $u = u(t)$ in (6) undergoes a duty cycle from $t = t_k$ to $t = t_{k+1} = t_k + \beta + T$, $k = 1, 2, \dots$, where the input is constant for an interval of length β (the burst phase) followed by an interval of length T with zero input (the coast phase), i.e.,

$$u(t) = \begin{cases} u_k & t_k \le t \le t_k + \beta \\ 0 & t_k + \beta < t < t_k + \beta + T \end{cases} \tag{18}$$

where u_k is given by (10) such that $u_k = u(v_k)$ where $v_k = -Ke(t)$.

The closed loop error system during the burst phase is given in (11). The solution to the system at the end of the burst phase of cycle k is

$$\mathbf{e}(t_k + \beta) = e^{\tilde{A}\beta}\mathbf{e}(t_k) \tag{19}$$

and the solution at the end of the coast phase is

$$\mathbf{e}(t_k + \beta + T) = e^{AT}\mathbf{e}(t_k + \beta) = e^{AT}e^{\tilde{A}\beta}\mathbf{e}(t_k). \tag{20}$$

Since the trace of $\tilde{A}$, see (13), is negative and the determinant is positive, its eigenvalues $(\lambda_1(\tilde{A}), \lambda_2(\tilde{A}))$ lie in the left half of the complex plane. Let $\tilde{\mathbf{v}}_1$ and $\tilde{\mathbf{v}}_2$ denote the corresponding eigenvectors. We have

$$e^{\tilde{A}\beta} = Ve^{\Lambda\beta}V^{-1}. \tag{21}$$

If the eigenvalues of $\tilde{A}$ are real, we have $V = [\tilde{\mathbf{v}}_1 \ \tilde{\mathbf{v}}_2]$ and $\Lambda = \text{diag}\{\lambda_1, \lambda_2\}$, which implies

$$e^{\Lambda\beta} = \begin{bmatrix} e^{\lambda_1 \beta} & 0 \\ 0 & e^{\lambda_2 \beta} \end{bmatrix}. \tag{22}$$

If the eigenvalues of $\tilde{A}$ are complex, let $\lambda_{1,2} = \alpha \pm i\gamma$ where $\alpha = \text{Re}\{\lambda(\tilde{A})\}$ and $\gamma = \text{Im}\{\lambda(\tilde{A})\}$. We have

$$V = \begin{bmatrix} \text{Re}\{\tilde{\mathbf{v}}_1\} & \text{Im}\{\tilde{\mathbf{v}}_1\} \\ \text{Re}\{\tilde{\mathbf{v}}_2\} & \text{Im}\{\tilde{\mathbf{v}}_2\} \end{bmatrix} \text{ and } \Lambda = \begin{bmatrix} \alpha & -\gamma \\ \alpha & \gamma \end{bmatrix} \tag{23}$$

which implies

$$e^{\Lambda\beta} = e^{\alpha\beta} \begin{bmatrix} \cos(\gamma\beta) & -\sin(\gamma\beta) \\ \sin(\gamma\beta) & \cos(\gamma\beta) \end{bmatrix} \tag{24}$$

Note, the eigenvalues of $e^{\tilde{A}\beta}$ (respectfully, e^{AT}) are $e^{\lambda_1(\tilde{A})\beta}$ and $e^{\lambda_2(\tilde{A})\beta}$ (respectfully, $e^{\lambda_1(A)T}$ and $e^{\lambda_2(A)T}$). A sufficient (but not necessary) condition for the composition of these two maps to exponentially stabilize the origin, is for all of the eigenvalues to be contained in the unit circle of the complex plane. Furthermore, $|e^{\lambda t}| < 1$ if and only if $\text{Re}\{\lambda\} < 0$ and $\text{Re}\{\lambda\} = 0$ implies $|e^{\lambda t}| = 1$. Therefore, since $\lambda_1(A) = \lambda_2(A) = 0$, and both eigenvalues of $\tilde{A}$ have negative real part, then the origin of the closed-loop system is exponentially stable.

Consider the case where $r = r(t)$ is a constant reference signal, $\dot{r} = \ddot{r} = 0$. The 2nd-order tracking error dynamics (6) simplify to

$$\dot{e}_2 = -\frac{D}{m}e_2 + \frac{1}{m}u. \tag{25}$$

The linear state-space form is

$$\dot{\mathbf{e}} = A_0\mathbf{e} + B_0 u, \tag{26}$$

where A_0 is given in (9) and $B_0 = [0; 1/m]$. This system is controllable because $\mathcal{C}_0 = \begin{bmatrix} B_0 & A_0 B_0 \end{bmatrix}$ is full rank: i.e.,

$$\mathcal{C}_0 = \begin{bmatrix} 0 & \frac{1}{m} \\ \frac{1}{m} & -\frac{D}{m^2} \end{bmatrix}. \tag{27}$$

The solution to this system at time t is

$$\mathbf{e}(t) = e^{A_0 t}\mathbf{e}(t_0) + \int_{t_0}^{t} e^{A_0 \tau} B_0 u(t-\tau)d\tau. \tag{28}$$

We have $A_0 = A_1 + A_2$, where

$$A_1 = \begin{bmatrix} 0 & 0 \\ 0 & -\frac{D}{m} \end{bmatrix} \text{ and } A_2 = \begin{bmatrix} 0 & 1 \\ 0 & 0 \end{bmatrix} \tag{29}$$

Note $A_1 A_2 = 0$, which implies A_1 and A_2 commute and $e^{A_0 t} = e^{(A_1 + A_2)t} = e^{A_1 t}e^{A_2 t}$.

Since A_1 is diagonal, it has eigenvalues 0 and $-\frac{D}{m}$ and, therefore,

$$e^{A_1 t} = \begin{bmatrix} 1 & 0 \\ 0 & e^{-\frac{D}{m}t} \end{bmatrix}. \tag{30}$$

Since $A_2^2 = 0$, we have

$$e^{A_2 t} = I + A_2 t = \begin{bmatrix} 1 & t \\ 0 & 1 \end{bmatrix}, \tag{31}$$

which implies

$$e^{A_0 t} = \begin{bmatrix} 1 & 0 \\ 0 & e^{-\frac{D}{m}t} \end{bmatrix} \begin{bmatrix} 1 & t \\ 0 & 1 \end{bmatrix} = \begin{bmatrix} 1 & t \\ 0 & e^{-\frac{D}{m}t} \end{bmatrix} \quad (32)$$

Suppose the input $u = u(t)$ undergoes a duty cycle as defined in (18) where the burst phase input is a constant, linear feedback control of the form $u_k = -K\mathbf{e}(t)$ with positive control gains $K = [K_1 \ K_2]$. The closed-loop system during the burst phase is

$$\dot{\mathbf{e}} = (A_0 - B_0 K)\mathbf{e} = \tilde{A}_0 \mathbf{e} \quad (33)$$

where

$$\tilde{A}_0 = \begin{bmatrix} 0 & 1 \\ -\frac{K_1}{m} & -\frac{D+K_2}{m} \end{bmatrix}. \quad (34)$$

The solution to the system at the end of the burst phase of cycle k is

$$\mathbf{e}(t_k + \beta) = e^{\tilde{A}_0 \beta} \mathbf{e}(t_k) \quad (35)$$

and, at the end of the coast phase,

$$\mathbf{e}(t_k + \beta + T) = e^{A_0 T} \mathbf{e}(t_k + \beta) = e^{A_0 T} e^{\tilde{A}_0 \beta} \mathbf{e}(t_k). \quad (36)$$

Since the trace of $\tilde{A}_0$ is negative and the determinant is positive, its eigenvalues $(\lambda_1(\tilde{A}_0), \lambda_2(\tilde{A}_0))$ lie in the left half of the complex plane. Furthermore, $|e^{\lambda t}| < 1$ if and only if $\text{Re}\{\lambda\} < 0$ and $\text{Re}\{\lambda\} = 0$ implies $|e^{\lambda t}| = 1$. Therefore, since $\lambda_1(A_0) = 0$, $\lambda_2(A_0) = -\frac{D}{m}$, and both eigenvalues of $\tilde{A}_0$ have negative real part, then the origin of the closed-loop system for tracking a constant reference signal is exponentially stable.

Fig 2 shows simulation results for the ideal vertical motion constant target case using intermittent actuation in comparison to continuous actuation. Fig 3 shows simulation results for the vertical motion constant target case where the control input is limited to the actual vertical thrust capability of the blimp.

B. Rotational reference tracking with intermittent actuation

Now consider tracking the angle of rotation about the vertical axis, where the state θ is mapped to the unit circle as $e^{i\theta}$ and thus has nonlinear dynamics. First, we will present an analysis for an arbitrary nonlinear system $x \in \mathbb{R}$ with intermittent burst-coast actuation, followed by the specific case for tracking the rotation θ.

Consider a nonlinear system $\dot{x} = f(x, u(t))$, $x \in \mathbb{R}$, with equilibrium point $f(x^*, 0) = 0$. Let $u = u(t)$ be an intermittent control input on a duty cycle from $t = t_k$ to $t = t_{k+1} = t_k + \beta + T$, $k = 1, 2, \ldots$, where the input is a function of x for the burst phase (interval of length β) followed by zero input for the coast phase (interval of length T), i.e.,

$$u(t) = \begin{cases} u(x) & t_k \le t \le t_k + \beta \\ 0 & t_k + \beta < t < t_k + \beta + T \end{cases} \quad (37)$$

Let $z = x - x^*$ so that the linearized open-loop system is $\dot{z} = Az$, where $A = \frac{\partial f}{\partial z}\Big|_{x=x^*}$. Let $g(x) = f(x, u(t))$ be the closed-loop system, with $g(x^*) = f(x^*, 0) = 0$ and
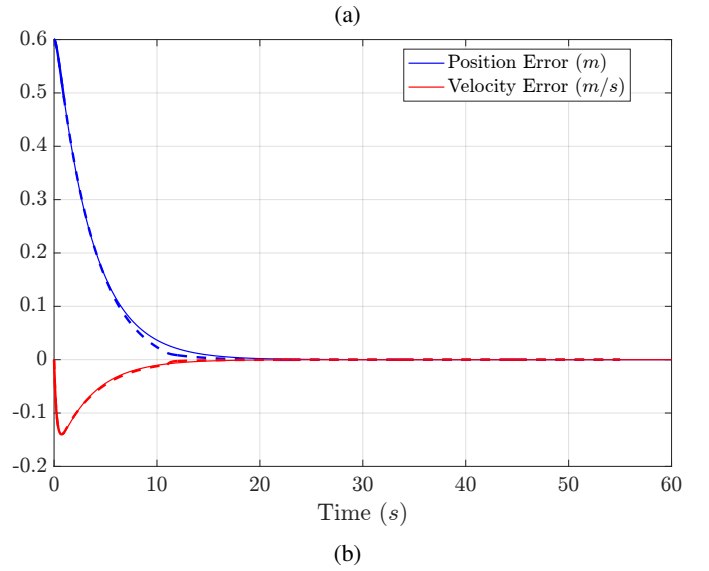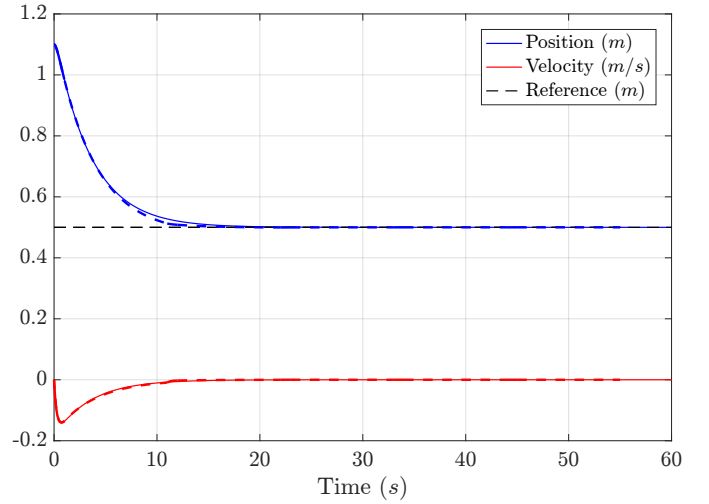

(a)

(b)

Fig. 2: Simulation results for tracking a constant vertical reference under ideal conditions with continuous actuation (thin, solid lines) and intermittent actuation (bold lines). The bold lines are solid for the active control burst phase and dashed for the passive coast phase.

linearization $\dot{z} = \tilde{A}z$, where $\tilde{A} = \frac{\partial g}{\partial z}\Big|_{x=x^*}$. The combined linearized intermittent burst-coast system is

$$\dot{z} = \begin{cases} \tilde{A}z & t_k \le t \le t_k + \beta \\ Az & t_k + \beta < t < t_k + \beta + T \end{cases} \quad (38)$$
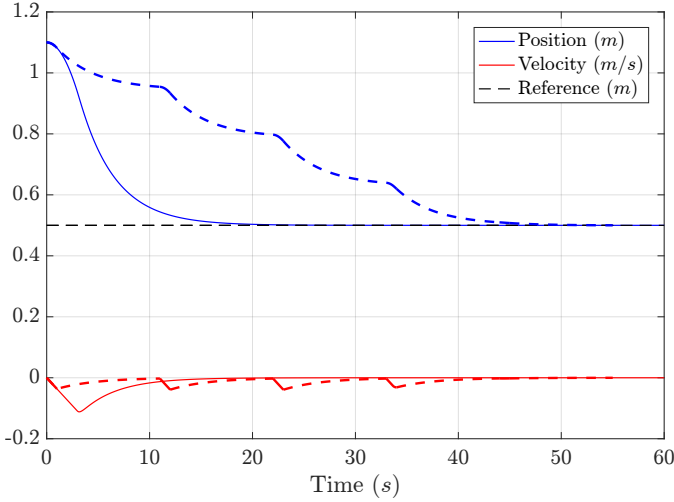
We have

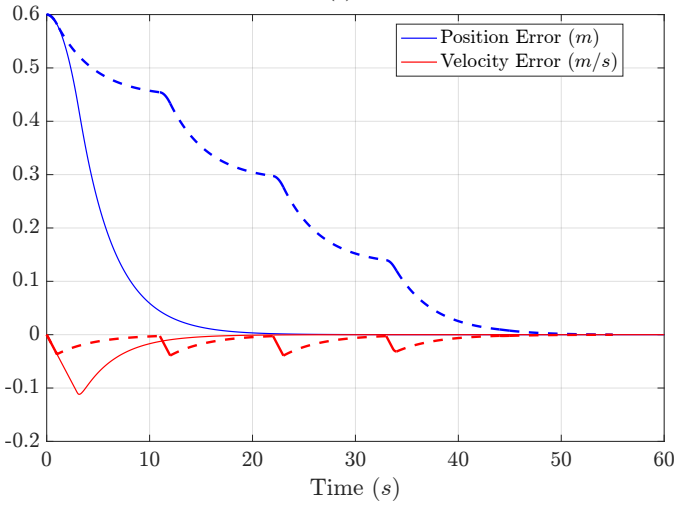$$z(t_k + \beta) = e^{\tilde{A}\beta} z(t_k) \quad (39)$$

and

$$z(t_{k+1}) = z(t_k + \beta + T) = e^{AT} z(t_k + \beta) \quad (40)$$

$$= e^{AT} e^{\tilde{A}\beta} z(t_k) \quad (41)$$

This is a composition of two linear maps. A sufficient condition for stability of the composed map is if $|\lambda(e^{AT})| \le 1$ and

Fig. 3: Simulation results for tracking a constant vertical reference subject to thrust constraints with continuous actuation (thin, solid lines) and intermittent actuation (bold lines). The bold lines are solid for the active control burst phase and dashed for the passive coast phase.

$|\lambda(e^{\tilde{A}\beta})| \leq 1$ we have $|\lambda(e^{AT})| = e^{\lambda(A)T}$ and $|\lambda(e^{\tilde{A}\beta})| = e^{\lambda(\tilde{A})\beta}$.

Let $\lambda(A) = \alpha \pm i\gamma$ and $\lambda(\tilde{A}) = \tilde{\alpha} \pm i\tilde{\gamma}$, which gives

$$|e^{\lambda(A)T}| = |e^{(\alpha \pm i\gamma)T}| = |e^{\alpha T}||e^{\pm i\gamma T}| \equiv e^{\alpha T}. \qquad (42)$$

Similarly, $|e^{\lambda(\tilde{A})\beta}| \equiv e^{\tilde{\alpha}\beta}$. Therefore, if $\alpha = Re(\lambda(A)) \leq 0$ and $\tilde{\alpha} = Re(\lambda(\tilde{\alpha})) \leq 0$, then the composed map is stable.

Consider the case where $Re(\lambda(A)) \not\leq 0$, i.e., the open-loop system is unstable. Note that $e^{AT}e^{\tilde{A}\beta} = e^{AT+\tilde{A}\beta}$ if and only if A and $\tilde{A}$ commute.

Eigenvectors $V = [v_1, \ldots, v_n]$ of A are also eigenvectors of e^{At}. If A has a full set of eigenvectors, and Λ is a diagonal matrix of eigenvalues $\lambda_i(A)$, $i = 1, \ldots, n$, then

$$e^{At} = Ve^{\Lambda t}V^{-1}, \qquad (43)$$

where $e^{\Lambda t}$ is a diagonal matrix of the eigenvalues of e^{At}. It follows that

$$\lambda_i(e^{At}) = e^{\lambda_i(A)t}. \qquad (44)$$

In the case where v is also an eigenvector of $\tilde{A}$, we have

$$\lambda(e^{AT}e^{\tilde{A}\beta}) = e^{\lambda(A)T}e^{\lambda(\tilde{A})\beta} \qquad (45)$$
$$= e^{\lambda(A)T+\lambda(\tilde{A})\beta}, \qquad (46)$$

where the sufficient condition for stability is $Re(\lambda(A)T + \lambda(\tilde{A})\beta) \leq 0$.

In the case where A and $\tilde{A}$ do not have the same eigenvectors, the spectral radius satisfies

$$\rho(e^{AT}e^{\tilde{A}\beta}) \leq \rho(e^{AT})\rho(e^{\tilde{A}\beta}), \qquad (47)$$

where

$$\rho(e^{AT}) = |\lambda_{\max}(e^{AT})| \qquad (48)$$
$$\leq |e^{\lambda_{\max}(A)T}| \qquad (49)$$
$$\leq e^{\alpha_{\max}(A)T} \qquad (50)$$

where $\alpha_{\max} > 0$ is the largest unstable open-loop eigenvalue. Similarly,

$$\rho(e^{\tilde{A}\beta}) = |\lambda_{\max}(e^{\tilde{A}\beta})| \qquad (51)$$
$$\leq |e^{\lambda_{\max}(\tilde{A})\beta}| \qquad (52)$$
$$\leq e^{\tilde{\alpha}_{\max}(\tilde{A})\beta} \qquad (53)$$

where $\tilde{\alpha}_{\max} < 0$ is the smallest stable closed-loop eigenvalue.

Substituting (50) and (53) into (47) yields the sufficient condition

$$\rho(e^{AT}e^{\tilde{A}\beta}) \leq e^{\alpha_{\max}(A)T+\tilde{\alpha}_{\max}(\tilde{A})\beta} \leq 1. \qquad (54)$$

Therefore, if $\alpha_{\max}(A)T+\tilde{\alpha}_{\max}(\tilde{A})\beta \leq 0$ the composed map is stable. This sufficient condition for stability of the composed map also applies to the linear system discussed in Section III-A, where $\alpha_{\max}(A) = 0$ and $\tilde{\alpha}_{\max}(\tilde{A}) < 0$ implies stability.

Now consider the specific case for tracking rotation about the vertical axis. Let $\boldsymbol{\theta} = (e^{i\theta}, \dot{\theta})$. The state dynamics for the 2nd-order system in (2) are mapped to the nonlinear state space form

$$\dot{\boldsymbol{\theta}} = \mathbf{f}(\boldsymbol{\theta}, u(t)), \qquad (55)$$

where

$$\mathbf{f}(\boldsymbol{\theta}, u(t)) = \begin{bmatrix} \theta_1\theta_2 \\ -\frac{D}{I_g}\theta_2 + \frac{1}{I_g}u(t) \end{bmatrix}. \qquad (56)$$

where u is a control input.

Let $r = r(t)$ denote a continuously differentiable time-varying reference signal with bounded derivatives, $\dot{r} = \dot{r}(t)$ and $\ddot{r} \equiv 0$, tracked by rotation about the vertical axis, and let $\boldsymbol{\varepsilon} = (\varepsilon_1, \varepsilon_2) = (e^{i(\theta-r)}, \dot{\theta} - \dot{r})$ denote the rotational tracking error, where ε_1 is constrained to the unit circle.

The nonlinear state space form is

$$\dot{\boldsymbol{\varepsilon}} = \mathbf{f}(\boldsymbol{\varepsilon}, u(t)), \qquad (57)$$

where

$$\mathbf{f}(\boldsymbol{\varepsilon}, u(t)) = \begin{bmatrix} \varepsilon_1 \varepsilon_2 \\ -\frac{D}{I_g}\varepsilon_2 + \frac{1}{I_g}u(t) \end{bmatrix}. \tag{58}$$

The open-loop system is linearized about the equilibrium point $\boldsymbol{\varepsilon}^* = (1,0)$ to get the matrix $A = \frac{\partial \mathbf{f}}{\partial \boldsymbol{\varepsilon}}\big|_{\boldsymbol{\varepsilon}^*}$, where the Jacobian is

$$\frac{\partial \mathbf{f}}{\partial \boldsymbol{\varepsilon}} = \begin{bmatrix} \varepsilon_2 & \varepsilon_1 \\ 0 & -\frac{D}{I_g} \end{bmatrix} \tag{59}$$

and the open-loop matrix is

$$A = \begin{bmatrix} 0 & 1 \\ 0 & -\frac{D}{I_g} \end{bmatrix}. \tag{60}$$

Let $u_k = -K\boldsymbol{\varepsilon}(t_k)$, which implies the closed-loop system $\dot{\boldsymbol{\varepsilon}} = \mathbf{g}(\boldsymbol{\varepsilon})$ is

$$\mathbf{g}(\boldsymbol{\varepsilon}, u(t)) = \begin{bmatrix} \varepsilon_1 \varepsilon_2 \\ -\frac{D}{I_g}\varepsilon_2 - \frac{1}{I_g}(K_1\varepsilon_1 + K_2\varepsilon_2) \end{bmatrix} \tag{61}$$

The closed-loop system is linearized about $\boldsymbol{\varepsilon}^*$ to get the matrix $\tilde{A} = \frac{\partial \mathbf{g}}{\partial \boldsymbol{\varepsilon}}\big|_{\boldsymbol{\varepsilon}^*}$, where the Jacobian is

$$\frac{\partial \mathbf{g}}{\partial \boldsymbol{\varepsilon}} = \begin{bmatrix} \varepsilon_2 & \varepsilon_1 \\ -\frac{K_1}{I_g} & -\frac{D+K_2}{I_g} \end{bmatrix}, \tag{62}$$

and the closed-loop matrix is

$$\tilde{A} = \begin{bmatrix} 0 & 1 \\ -\frac{K_1}{I_g} & -\frac{D+K_2}{I_g} \end{bmatrix}. \tag{63}$$

Since the trace of $\tilde{A}$ is negative and the determinant is positive, its eigenvalues $(\lambda_1(\tilde{A}), \lambda_2(\tilde{A}))$ lie in the left half of the complex plane. Therefore the closed loop continuous-time error system stabilizes $\boldsymbol{\varepsilon}^*$.

Suppose $u = u(t)$ in (57) is an intermittent control input on a duty cycle from $t = t_k$ to $t = t_{k+1} = t_k + \beta + T$, $k = 1, 2, \ldots$, where the input is a function of ε for the burst phase (interval of length β) followed by zero input for the coast phase (interval of length T), i.e.,

$$u(t) = \begin{cases} u(\varepsilon) & t_k \le t \le t_k + \beta \\ 0 & t_k + \beta < t < t_k + \beta + T \end{cases} \tag{64}$$

The combined linearized intermittent burst-coast system is

$$\dot{\boldsymbol{\varepsilon}} = \begin{cases} \tilde{A}\boldsymbol{\varepsilon} & t_k \le t \le t_k + \beta \\ A\boldsymbol{\varepsilon} & t_k + \beta < t < t_k + \beta + T \end{cases} \tag{65}$$

The solution to this system at time t_{k+1} is the composition of two linear maps.

We have solutions to this system at time $t_k + \beta$

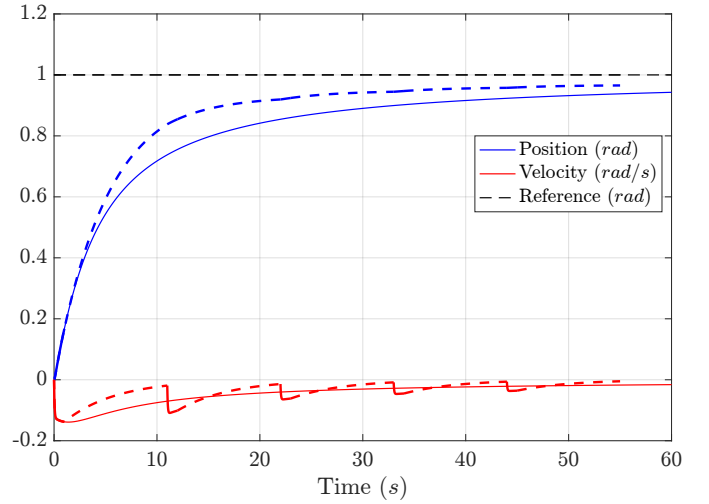$$\boldsymbol{\varepsilon}(t_k + \beta) = e^{\tilde{A}\beta}\boldsymbol{\varepsilon}(t_k) \tag{66}$$
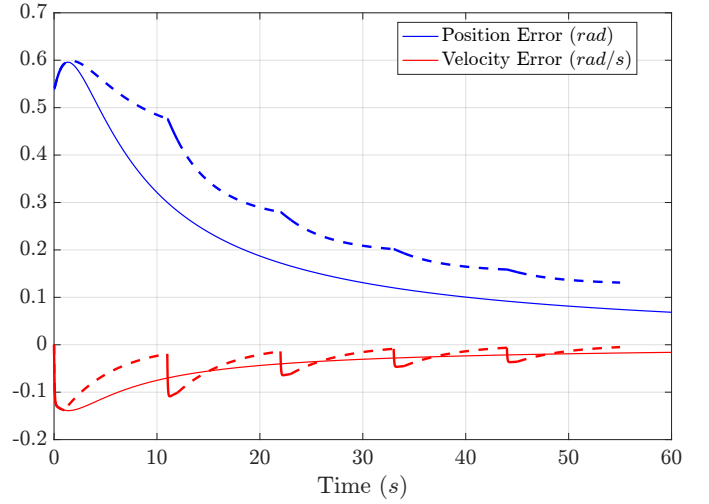
and t_{k+1}

$$\boldsymbol{\varepsilon}(t_{k+1}) = \boldsymbol{\varepsilon}(t_k + \beta + T) = e^{AT}\boldsymbol{\varepsilon}(t_k + \beta) \tag{67}$$

$$= e^{AT}e^{\tilde{A}\beta}\boldsymbol{\varepsilon}(t_k) \tag{68}$$

The sufficient condition for stability follows from (42). Since $\alpha = \mathrm{Re}(\lambda_{1,2}(A)) \le 0$ and $\tilde{\alpha} = \mathrm{Re}(\lambda(\tilde{A})) < 0$, the composed map is stable.

(a)

(b)

Fig. 4: Simulation results for tracking a constant angle reference under ideal conditions with continuous actuation (thin, solid lines) and intermittent actuation (bold lines). The bold lines are solid for the active control burst phase and dashed for the passive coast phase.

Fig. 4 shows simulation results for the ideal rotational motion constant target case using intermittent actuation in comparison to continuous actuation. Fig. 5 shows simulation results for the rotational motion constant target case where the control input is limited to the actual torque capability of the blimp.

The ideal rotational case without torque constraints gets within 0.1 radians of the target angle in only 5 burst-coast cycles, but with the torque limited to the physical blimp constraint it only gets within 0.2 radians in 5 cycles. The rotational case needs over 20 burst-coast cycles to converge within 0.1 radians without changing the relative lengths of the burst and coast phases. It is part of ongoing work to more accurately characterize the rotational drag model used for these
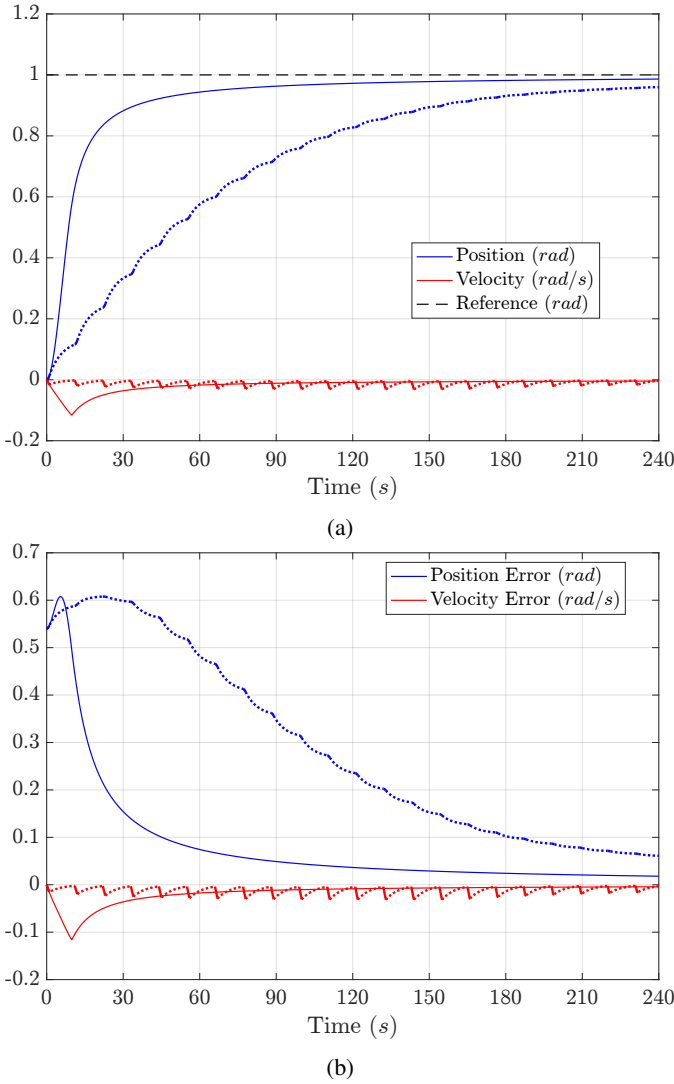
(a)

(b)

Fig. 5: Simulation results for tracking a constant angle reference subject to thrust constraints with continuous actuation (thin, solid lines) and intermittent actuation (bold lines). The bold lines are solid for the active control burst phase and dashed for the passive coast phase.

IV. EXPERIMENTAL RESULTS

For each MAB experiment the blimp envelope is inflated with helium and the gondola is ballasted for the blimp to be neutrally buoyant. The experiments use a constant vertical reference of 0.8 meters and compare the performance of

the blimp using continuous control and intermittent actuation control.

Fig. 6 contains results for the vertical motion experiments. Figs. 6a and 6b show position and error results, respectively, for tracking a constant reference altitude with continuous actuation using the existing control described in Section II and with intermittent actuation using the control law derived in Section III-A. The discrepancy between the continuous actuation experimental and simulation results indicates that the MAB was balanced positively buoyant instead of neutrally buoyant. For the intermittent actuation test, the MAB was re-balanced to be slightly negatively buoyant.
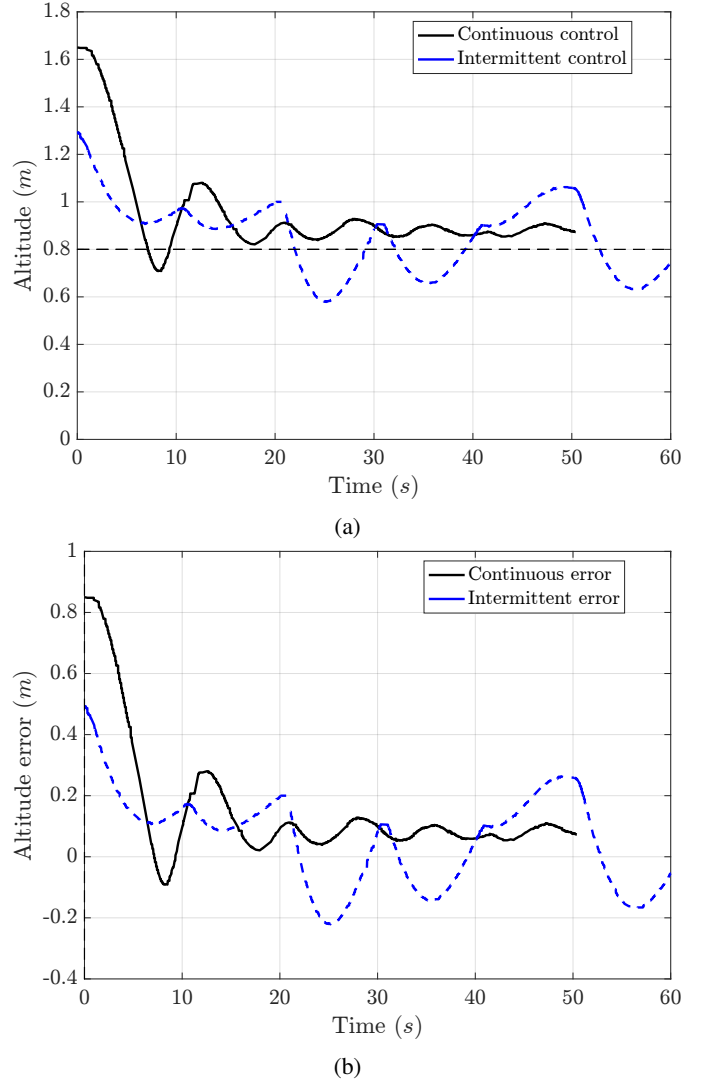

(a)

(b)

Fig. 6: Experimental results of tracking constant vertical position with the miniature autonomous blimp. The lines are solid for the active control 'burst' phase, and dashed for the passive 'coast' phase. The corresponding position tracking error has standard deviation $\sigma = 0.2000m$ and $\sigma = 0.1451m$, for continuous actuation and intermittent actuation, respectively.

The overall error variance is larger for the continuous actuation test because it started from a higher initial altitude.

dynamics and to determine appropriate interval lengths of the rotational burst-coast cycle to ensure exponential stability. However, the vertical motion cases are able to converge to the target position in simulation with both ideal thrust and with the thrust limited to the physical blimp constraints. The next section presents experimental results for vertical motion intermittent actuation.

However, looking at the tracking error after a proximity threshold of 0.2 meters is reached, the standard deviation is $\sigma = 0.0668m$ for continuous actuation, and $\sigma = 0.1331m$ for intermittent actuation. While continuous actuation is able to hold position more precisely, Fig. 7 compares the amount of vertical thrust used for continuous and intermittent actuation.
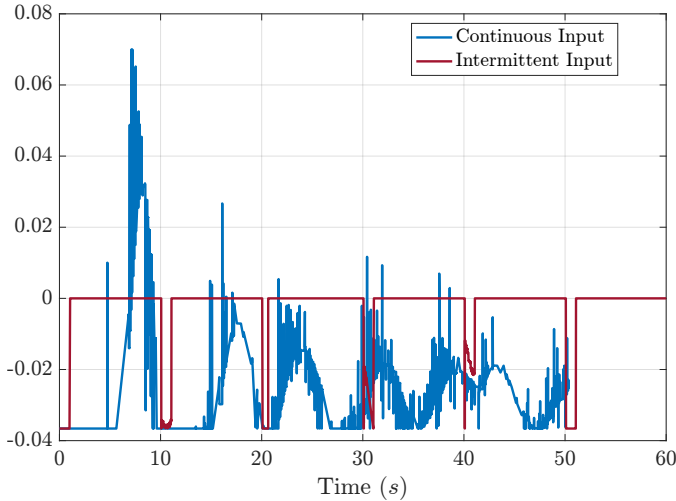

Fig. 7: Control input force for tracking a constant vertical reference with continuous actuation and intermittent burst-coast actuation.

V. Conclusion

This work presents an intermittent control strategy for tracking a time-varying target reference with theoretically proven stability. The error-based tracking method with state-feedback control is demonstrated in simulation for decoupled 1-DOF vertical and rotational motion tracking a constant target. Experimental results for vertical motion tracking a constant target reference compares performance between continuous and intermittent actuation using the MAB. Ongoing work aims to improve the dynamical model by refining the physical parameters and optimizing the burst and coast interval lengths for each 1-DOF motion case, as well as expansion of the model to coupled 2-DOF planar motion. Future work seeks to further develop the intermittent control strategy to include state estimation and onboard measurements for estimation of the target trajectory. The model could also be expanded to a multi-agent approach for cooperative target localization and tracking.

References

[1] D. L. Kramer and R. L. McLaughlin, "The behavioral ecology of intermittent locomotion," *American Zoologist*, vol. 41, no. 2, pp. 137–153, 2001.

[2] Y. Aidan, I. Bleichman, and A. Ayali, "Pausing to swarm: locust intermittent motion is instrumental for swarming-related visual processing," *Biology Letters*, vol. 20, no. 2, p. 20230468, 2024.

[3] P. Paoletti and L. Mahadevan, "Intermittent locomotion as an optimal control strategy," *Proceedings of the Royal Society A: Mathematical, Physical and Engineering Sciences*, vol. 470, no. 2164, p. 20130535, 2014.

[4] A. A. Thompson, L. Cañuelas, and D. A. Paley, "Estimation and control for collective motion with intermittent locomotion," in *American Control Conference (ACC)*, 2022, pp. 747–754.

[5] A. A. Thompson, L. Cañuelas, and D. A. Paley, "Phase synchronization with intermittent locomotion and non-overlapping sensing and actuation," *IEEE Transactions on Automatic Control*, 2023.

[6] A. Hu, J. H. Park, and M. Hu, "Consensus of nonlinear multiagent systems with intermittent dynamic event-triggered protocols," *Nonlinear Dynamics*, vol. 104, pp. 1299–1313, 2021.

[7] K. Chen, J. Wang, Y. Zhang, and Z. Liu, "Second-order consensus of nonlinear multi-agent systems with restricted switching topology and time delay," *Nonlinear Dynamics*, vol. 78, no. 2, pp. 881–887, 2014.

[8] X. Liu, J.-W. Xiao, D. Chen, and Y.-W. Wang, "Dynamic consensus of nonlinear time-delay multi-agent systems with input saturation: an impulsive control algorithm," *Nonlinear Dynamics*, vol. 97, pp. 1699–1710, 2019.

[9] E. J. Berkenpas, C. M. Shepard, R. J. Suitor, P. Zaidins, D. A. Paley, and K. Abernathy, "Swarming Driftcams: a novel platform for locating and tracking pelagic scattering layers," in *OCEANS 2021: San Diego - Porto*, San Diego, CA, 2021, pp. 1–6.

[10] E. J. Berkenpas, B. S. Henning, C. M. Shepard, A. J. Turchik, C. J. Robinson, E. J. Portner, D. H. Li, P. C. Daniel, and W. F. Gilly, "A buoyancy-controlled Lagrangian camera platform for in situ imaging of marine organisms in midwater scattering layers," *IEEE Journal of Oceanic Engineering*, vol. 43, no. 3, pp. 595–607, July 2018. [Online]. Available: https://ieeexplore.ieee.org/document/8026568/

[11] R. J. Suitor, E. Berkenpas, and D. A. Paley, "Dynamics and Control of a Buoyancy-Driven Underwater Vehicle for Estimating and Tracking the Scattering Layer," *IEEE Robotics and Automation Letters*, vol. 8, no. 5, pp. 3015–3022, May 2023.

[12] Q. Tao, "Design and control of an indoor miniature autonomous blimp," Ph.D. dissertation, Georgia Institute of Technology, 2020.

[13] T. X. Lin, M. Rossouw, A. B. Maxseiner, T. Schuler, M. A. Garratt, S. Ravi, F. Zhang, D. M. Lofaro, and D. A. Sofge, "Miniature autonomous blimps for indoor applications," in *AIAA SCITECH 2022 Forum*, 2022, p. 1834.

[14] T. Schuler, D. M. Lofaro, L. McGuire, A. Schroer, T. Lin, and D. Sofge, "A study of robotic swarms and emergent behaviors using 25+ realworld lighter-than-air autonomous agents (lta3)," in *3rd International Symposium on Swarm Behavior and Bio-Inspired Robotics (SWARM)*, 2019.

[15] T. I. Fossen, *Handbook of marine craft hydrodynamics and motion control*. Chichester, West Sussex: Wiley, 2011.

[16] Q. Tao, M. Hou, and F. Zhou, "Modeling and identification of coupled translational and rotational motion of underactuated indoor miniature autonomous blimps," in *16th International Conference on Control, Automation, Robotics and Vision (ICARCV)*, 2020, pp. 339–344.

[17] Q. Tao, J. Cha, M. Hou, and F. Zhang, "Parameter identification of blimp dynamics through swinging motion," in *15th International Conference on Control, Automation, Robotics and Vision (ICARCV)*. IEEE, 2018, pp. 1186–1191.

[18] Q. Tao, T. J. Tan, J. Cha, Y. Yuan, and F. Zhang, "Modeling and control of swing oscillation of underactuated indoor miniature autonomous blimps," *Unmanned Syst.*, vol. 9, no. 1, pp. 73–86, 2021.

ADDITIONAL FIGURES

This appendix includes additional figures from experiments and simulation.

Fig. 8 shows experimental results for tracking a constant vertical reference with continuous actuation for a) test C1 30 seconds and b) test C2 35 seconds. Error standard deviation for c) test C1 $\sigma = 0.1444m$ and d) test C2 $\sigma = 0.0905m$. Control input force f_z for e) test C1 and f) test C2.

Fig. 9 shows experimental results for tracking a constant vertical reference with intermittent burst-coast actuation for a) test I2, b) test I3, and c) test I8, where the solid line represents the burst phase and the dashed line represents the coast phase. The tracking error has standard deviation of d) test I2 $\sigma = 0.1670m$, e) test I3 $\sigma = 0.1879m$, and f) test I8 $\sigma = 0.1739m$. Control input force f_z for g) test I2, h) test I3, and i) test I8.

Fig. 10 shows experimental results for tracking a constant vertical reference with a) continuous actuation for test C3 and b) intermittent burst-coast actuation for test I9, where the solid line represents the burst phase and the dashed line represents the coast phase. The tracking error has standard deviation of c) test C3 $\sigma = 0.2000m$ and d) test I9 $\sigma = 0.1451m$. Control input force f_z for e) test C3, f) test I9.
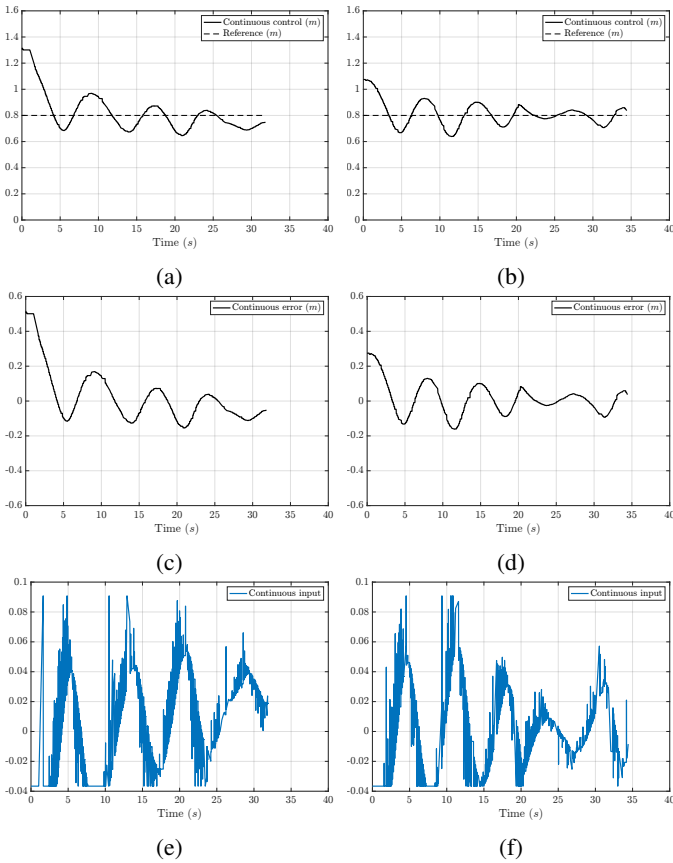

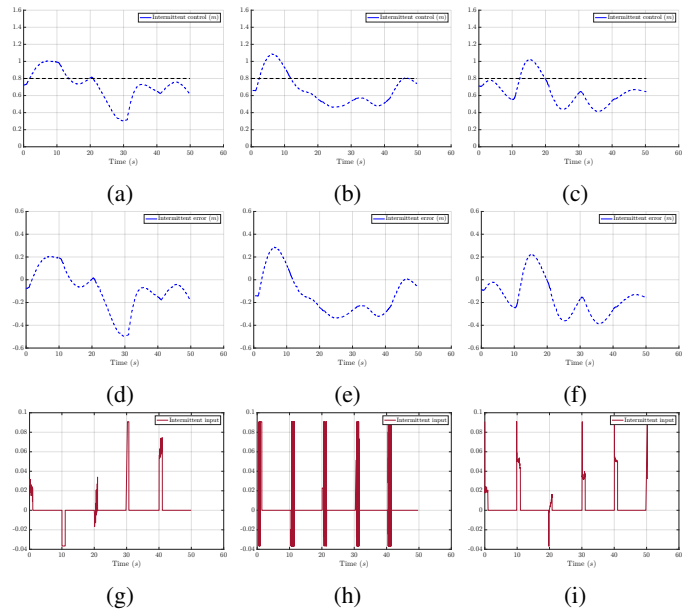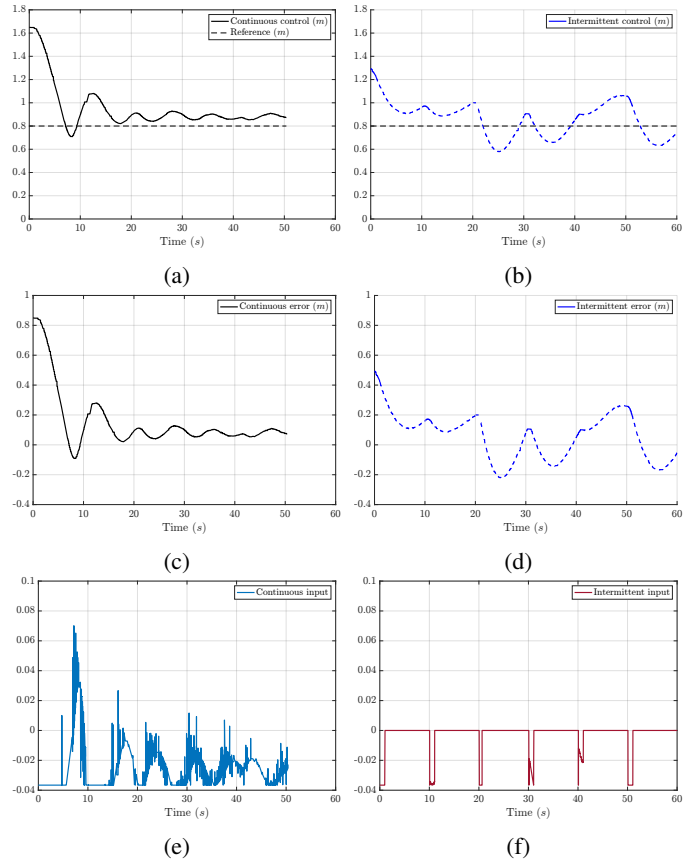Fig. 9: Additional intermittent tests

Fig. 8: Additional continuous tests

Fig. 10: Individual results compared in section IV